Acta Crystallographica Section D
Biological Crystallography
ISSN 0907-4449

Crystallization of 4-hydroxybenzoyl-CoA reductase and the structure of its electron donor ferredoxin

Mihaela Unciuleac,[a] Matthias Boll,[a] Eberhard Warkentin[b] and Ulrich Ermler[b]*

[a]Institut für Biologie II, Mikrobiologie, Schänzlestrasse 1, D-79104 Freiburg, Germany, and [b]Max-Planck-Institut für Biophysik, Marie-Curie-Strasse 15, D-60439 Frankfurt, Germany

Correspondence e-mail: ulrich.ermler@mpibp-frankfurt.mpg.de

Received 7 October 2003
Accepted 10 December 2003

PDB Reference: ferredoxin TaFd, 1rgv, 1rgvsf.

4-Hydroxybenzoyl-CoA reductase (4-HBCR) is a central enzyme in the metabolism of phenolic compounds in anaerobic bacteria. The enzyme catalyzes the reductive removal of the phenolic hydroxyl group from 4-hydroxybenzoyl-CoA, yielding benzoyl-CoA and water. 4-HBCR belongs to the xanthine oxidase (XO) family of molybdenum enzymes which occur as heterodimers, $(\alpha\beta\gamma)_2$. 4-HBCR contains two molybdopterins, four [2Fe–2S] and two [4Fe–4S] clusters and two FADs. A low-potential *Allochromatium vinosum*-type ferredoxin containing two [4Fe-4S] clusters serves as an *in vivo* electron donor for 4-HBCR. In this work, the oxygen-sensitive proteins 4-HBCR and the ferredoxin (TaFd) from *Thauera aromatica* were crystallized under anaerobic conditions. 4-HBCR crystallized with PEG 4000 and MPD as precipitant diffracted to about 1.6 Å resolution and the crystals were highly suitable for X-ray structure analysis. Crystals of TaFd were obtained with $(NH_4)_3PO_4$ as precipitant and revealed a solvent content of 77%, which is remarkably high for a small soluble protein. The structure of TaFd was solved at 2.9 Å resolution by the molecular-replacement method using the highly related structure of the ferredoxin (CvFd) from *A. vinosum* as a model. Structural changes between the two ferredoxins around the [4Fe–4S] cluster can be correlated with their different redox potentials.

1. Introduction

The degradation of aromatic compounds has long been considered as a unique domain of aerobic organisms; key reactions in the aromatic metabolism are catalyzed by mono- or dioxygenases. However, in recent years a number of anaerobic bacteria have been identified which are able to use various aromatic compounds as their sole source of energy and cell carbon (Boll *et al.*, 2002; Gibson & Harwood, 2002). In the absence of oxygen, the dearomatization process is catalyzed by ring reductases. For example, the key enzyme benzoyl-CoA reductase (BCR, dearomatizing) catalyzes the two-electron reduction of benzoyl-CoA to a non-aromatic cyclic diene using a low-potential ferredoxin as electron donor (Boll *et al.*, 2000; Boll & Fuchs, 1998; Fig. 1). A further important reaction is catalyzed by 4-hydroxybenzoyl-CoA reductase (4-HBCR, dehydroxylating). It plays an important role in the anaerobic metabolism of phenolic compounds, catalyzing the reductive removal of the *para*-hydroxyl group and yielding benzoyl-CoA and water (Fig. 1; Brackmann & Fuchs, 1993). The dimeric enzyme has a molecular weight of 275 kDa; each monomer consists of three subunits with molecular weights 85, 35 and 17 kDa, resulting in an $(\alpha\beta\gamma)_2$ composition (Brackmann & Fuchs, 1993). The enzyme contains two $[2Fe–2S]^{+1/+2}$ and one $[4Fe–4S]^{+1/+2}$ cluster, one FAD and one molybdopterin cofactor per $\alpha\beta\gamma$ monomer (Boll *et al.*, 2001). Amino-acid sequence analysis revealed similarities (27–47% identity for the different subunits) to members of the xanthine oxidase (XO) family

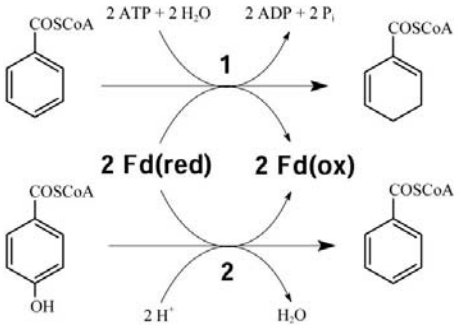

Figure 1
Reactions catalyzed by benzoyl-CoA reductase (1) and 4-hydroxybenzoyl-CoA reductase (2). In *T. aromatica*, reduced ferredoxin serves as *in vivo* electron donor for both reactions; it is regenerated by 2-oxoglutarate: ferredoxin oxidoreductase.

of Mo-containing hydroxylases and to the Mo- and Cu-containing CO dehydrogenases from aerobic organisms (Breese & Fuchs, 1998). Several features distinguish the oxygen-sensitive 4-HBCR from all other members of the XO family of Mo enzymes: (i) 4-HBCR catalyzes the irreversible reverse reaction of the XO-family enzymes, the dehydroxylation of the phenolic moiety of the substrate (in contrast, all XO enzymes oxidize their substrates using water as hydroxyl donor); (ii) a one-electron transfer mechanism to the substrate by means of highly reactive radical species has been proposed for the 4-HBCR reaction (Buckel & Keese, 1995), whereas the typical hydroxylation reactions of XO members are assumed to involve a two-electron transfer from the substrate to the Mo-cofactor; (iii) 4-HBCR is the only member of the XO family that harbours an additional low-potential [4Fe–4S]$^{+1/+2}$ cluster that is considered to play a crucial role in the reductive catalysis.

In *Thauera aromatica*, the electron donor for both 4-HBCR and benzoyl-CoA reductase (BCR) was identified to be a 9.7 kDa ferredoxin (TaFd; Boll & Fuchs, 1998). Recently, a 2-oxoglutarate:ferredoxin oxidoreductase has been identified in *T. aromatica* that regenerates reduced ferredoxin (Dörner & Boll, 2002). The gene coding for TaFd is located adjacent to the four structural genes of BCR (Breese *et al.*, 1998). TaFd belongs to the *Allochromatium vinosum* type of ferredoxins containing two [4Fe–4S]$^{+1/+2}$ clusters and shows 52% amino-acid sequence identity to the *A. vinosum* (previously termed *Chromatium vinosum*) ferredoxin (CvFd) (Moulis *et al.*, 1996). With a molecular weight of ∼10 kDa, this type is distinguished from the clostridial type (∼6 kDa) by a six amino-acid insertion between two cysteines of the typical C*xx*C*xx*C . . . CP sequence motif of the C-terminal [4Fe–4S] cluster and by an extended C-terminus. The crystal structure of CvFd revealed a different protein environment for the two [4Fe–4S]$^{+1/+2}$ clusters which allows a distinction to be made between the N-terminal cluster (referred to as cluster I) and the C-terminal cluster (cluster II) (Moulis *et al.*, 1996). In contrast, the environment of the clusters of clostridial ferredoxins is rather similar. As a consequence, the two [4Fe–4S]$^{+1/+2}$ clusters of the clostridial type have comparable redox potentials (∼−400 mV), whereas the two [4Fe–4S]$^{+1/+2}$ clusters in *C. vinosum*-type ferredoxins have very different redox potentials: *e.g.* −460 mV (cluster II) and −655 mV (cluster I) for CvFd (Kyritsis *et al.*, 1998) and −431 mV (cluster II) and −585 mV (cluster I) for TaFd (Boll *et al.*, 2000). The physiological impact of the differing redox potentials is not yet known. So far, TaFd is the only Cv-type ferredoxin for which both the natural electron-donating and electron-accepting enzymes are known. The clusters of TaFd also exhibit unusual electron paramagnetic resonance features: the cluster with the more positive redox potential displayed spectra corresponding to an S = 3/2 and S = 5/2 spin mixture, whereas the low-potential cluster exhibited a spectrum corresponding to a typical S = 1/2 [4Fe–4S]$^{+1/+2}$ cluster (Boll *et al.*, 2000).

In this work, 4-HBCR from *T. aromatica* and its electron donor ferredoxin were anaerobically crystallized for the first time. The structure of TaFd was determined at 2.9 Å resolution.

Table 1
Crystallographic and refinement data of ferredoxin and 4-HBCR from *T. aromatica*.

Values in parentheses are for the last resolution shell.

		4-HBCR	
	Ferredoxin	Crystal form 1	Crystal form 2
Space group	$P3_121$	$P2_12_12_1$	$P2_12_12_1$
Unit-cell parameters			
a (Å)	79.0	116.6	112.9
b (Å)		150.2	152.3
c (Å)	49.3	175.3	174.6
No. of molecules per AU	1	1	1
Solvent content (%)	77	58	58
Resolution (Å)	2.9 (3–2.9)	2.5 (2.6–2.5)	1.7 (1.8–1.7)
R_{sym} (%)	8.1 (37)	6.7 (33)	8.1 (33)
$I/\sigma(I)$	12.4 (2.7)	19.2 (3.5)	13.2 (2.3)
Completeness (%)	95.7 (70)	99.5 (97.4)	97.0 (93.6)
No. reflections	3753	103628	318643
Multiplicity	2.9	4.5	3.1
Solution method	MR		
R_{cryst} (%)	19.7 (33)		
R_{free} (%)	21.9 (25)		
R.m.s.d. bonds (Å)	0.007		
R.m.s.d. angles (°)	1.22		
Average B (Å^2)	49		
Residues per AU	80		
Ligands per AU	2 Fe_4S_4		

2. Materials and methods

2.1. Growth of bacterial cells and protein purification

T. aromatica (DSM 6984) was grown anaerobically at 301 K in a mineral salt medium. 4-Hydroxybenzoate and nitrate in a ratio of 1:3.5 were used as the sole sources of cell carbon and energy. Continuous feeding of the substrates, cell harvesting, storage and preparation of cell extracts were performed as described previously (Tschech & Fuchs, 1987). Purification of 4-HBCR and ferredoxin from extracts of *T. aromatica* was performed under strictly anaerobic conditions in a glove box under an N_2/H_2 atmosphere (95:5 by volume) as described previously (Brackmann & Fuchs, 1993; Boll & Fuchs, 1998).

2.2. Crystallization and data collection

Crystallization trials for 4-HBCR and TaFd were performed with the hanging-drop and sitting-drop vapour-diffusion methods under strictly anaerobic conditions in the glove box. Initial screenings at 281 and 293 K were made with the commercial Hampton Research Crystal Screen kits I and II (Jancarik & Kim, 1991) and the Jena Bioscience kit. X-ray diffraction measurements were performed at the ID14-4 beamline at ESRF in Grenoble and in-house using a MAR Research imaging-plate detector mounted on a Rigaku RU-200 X-ray generator fitted with Osmic confocal optics and a copper target (λ = 1.542 Å). Data were processed with *DENZO*, *SCALEPACK* (Otwinowski & Minor, 1997) and *CCP*4 programs (Collaborative Computational Project, Number 4, 1994).

2.3. Phase determination and model refinement

The phases of TaFd were determined by the molecular-replacement method using *EPMR* (Kissinger *et al.*, 1999) for calculation and the structure of the two-[4Fe–4S] ferredoxin from *A. vinosum* (Moulis *et al.*, 1996) as a model. Incorporation of the primary structure of TaFd (Breese *et al.*, 1998) and model building was performed within *O* (Jones *et al.*, 1991). The structure was refined using *CNS* (Brünger *et al.*, 1998), applying standard protocols. Model errors were assessed with the programs *CNS*, *PROCHECK* (Laskowski *et al.*, 1993) and *WHAT CHECK* (Hooft *et al.*, 1996).

3. Results and discussion

3.1. Crystallization of 4-hydroxybenzoyl-CoA reductase (4-HBCR)

For performing crystallization experiments, 4-HBCR was concentrated to 15–20 mg ml^{-1} and stored in 5 m*M* triethanolamine, 2 m*M* $MgCl_2$ and 2 m*M* dithionite pH 7.8. Stacks of small plate-shaped crystals grew using polyethylene glycols (PEG) of various molecular weight as precipitant. Optimal conditions were found at 303 K by

mixing 2.5 µl of protein solution and 2.5 µl of reservoir solution containing 10%(*w*/*v*) PEG 4000, 15%(*w*/*v*) 2-methyl-2,4-pentanediol and 0.1 *M* HEPES pH 7.5. 4-HBCR crystallized in two different forms, both of which adopted space group $P2_12_12_1$. (The merging *R* value between two data sets was 50% in the resolution range 5–10 Å.) The unit-cell parameters of crystal forms 1 and 2 were determined to be $a = 116.6$, $b = 150.2$, $c = 175.3$ Å and $a = 112.9$, $b = 152.3$, $c = 174.6$ Å, respectively, and the crystals diffracted to resolutions of about 2 and 1.6 Å, respectively; see also Table 1. The volume-to-weight ratio V_M is 2.8 Å^3 Da^{-1} (Matthews, 1968), assuming the presence of one $(\alpha\beta\gamma)_2$ heterodimer in the asymmetric unit; the corresponding solvent content is 58%. All measurements were achieved under flash-cooling conditions after soaking the crystals in a cryoprotectant solution containing 5%(*w*/*v*) PEG 4000, 20%(*w*/*v*) MPD and 0.2 *M* HEPES pH 7.5. Diffraction data from crystal form 2 were collected at beamline ID14-4. Of the 1 218 419 reflections measured, 606 220 were unique. The completeness of the data was 94% and the R_{sym} value was 7.6% in the resolution range 1.7–40.0 Å.

The determination of the phases of 4-HBCR is under way by collecting MAD data at the iron edge. An alternative possibility might be molecular replacement using, for example, the CO dehydrogenase of *Oligotropha corboxidovorans* (PDB code 1qj2; overall sequence identity 31%) as a model.

3.2. Ferredoxin (TaFd)

3.2.1. Structure determination. Brown single crystals of protein were formed after three weeks at 281 K in a drop consisting of 2.5 µl enzyme solution (5.8 mg ml^{-1}) and 2.5 µl reservoir buffer. The reservoir buffer consisted of 100 m*M* sodium citrate pH 5.8 and 1.8 *M* ammonium phosphate. TaFd crystals were mounted in 0.7 mm diameter glass capillaries and diffraction data were collected in-house at 2.9 Å resolution at a temperature of 283 K. The space group was determined to be $P3_121$ and the unit-cell parameters were $a = 79.0$, $c = 49.3$ Å. The Matthews parameter V_M of 5.0 Å^3 Da^{-1} suggested the presence of two to three molecules in the asymmetric unit (Matthews, 1968). Remarkably, the molecular-replacement solution was complete with only one molecule per asymmetric unit. The corresponding solvent content of about 77% is very unusual for a small soluble protein. During refinement, the *R* and R_{free} factors fell to final values of 19.7 and 21.9%, respectively, in the resolution range 40–2.9 Å. The resulting model includes amino acids 1–80 and two [4Fe–4S] clusters. The bond-length and bond-angle deviations from the standard geometry were 0.007 Å and 1.2°, respectively; no residues were in forbidden regions of the Ramachandran plot (Ramachandran & Sasisekharan, 1968). Solvent molecules were not included owing to the limited resolution of the diffraction data.

3.2.2. Structure analysis. TaFd is composed of an N-terminal core domain with the typical fold of [4Fe–4S] ferredoxins (Adman *et al.*, 1973) and a C-terminal extension. In the ferredoxin fold, the two [4Fe–4S] clusters are sandwiched between a layer consisting of four roughly parallel strands, two of them forming a short sheet and a layer built up of two irregular segments containing small pieces of helical character (Fig. 2*a*). The structure of TaFd is very similar to that of the *A. vinosum* enzyme (CvFd), with the r.m.s. deviation of the C^α atoms being about 0.5 Å. CvFd contained two significant structural differences compared with clostridial [4Fe–4S] ferredoxins (Moulis *et al.*, 1996; see above). Both, the six-residue insertion in the typical C*xx*C*xx*C...CP sequence motif located between the two iron-ligating cysteines and the 3.5-turn α-helix at the C-terminal end were also found in TaFd. Conformational deviations between TaFd and CvFd of greater than 1.5 Å are only observed in loop regions, where the structure is influenced by different crystal packing. The protein surfaces of both TaFd and CvFd are characterized by an excess of negatively charged residues. This dominance is particularly striking at the protein surface enveloping cluster I, such that binding of TaFd to a positively charged patch at the surface of 4-HBCR and BCR appears to be likely. As both 4-HBCR and BCR require electrons at a very low potential for the reactions catalyzed, an interaction with the more negative cluster I seems favourable for efficient interprotein electron transfer.

The protein scaffold that contacts the [4Fe–4S] clusters is fairly conserved between TaFd and CvFd. This is qualitatively reflected in the very negative redox potential of cluster I (−585 mV for TaFd and −665 mV for CvFd) and the less negative potential (−431 mV for TaFd and −460 mV for CvFd) of cluster II. The highly similar backbone of these two enzymes implies that the differences in their redox potential must arise from local amino-acid exchanges adjacent to the Fe/S clusters. The side chains contacting cluster II are identical except for Pro47, which is replaced by a serine in CvFd; in both cases the C^β atom contacts the cluster. The significant difference of 70 mV in the redox potential between clusters I of TaFd and CvFd may arise from an exchange of Thr10 for isoleucine and of Ala14 for valine. The more hydrophobic environment of cluster I in CvFd (Fig. 2*b*) favours the reduced state, as the higher positive charge density at the iron of the oxidized state can be better compensated for by more polar residues. This argument is supported by a 50 mV increased redox potential of a V14G mutant of CvFd (Kyritsis *et al.*, 1998). Val14 might play an additional role by shielding the [4Fe–4S] cluster from the bulk solvent. Moreover, the I40N and L44S mutants of *Azotobacter vinelandii* (Chen *et al.*, 2002), which correspond to positions 10 and 14 in TaFd, increase the redox potential by nearly

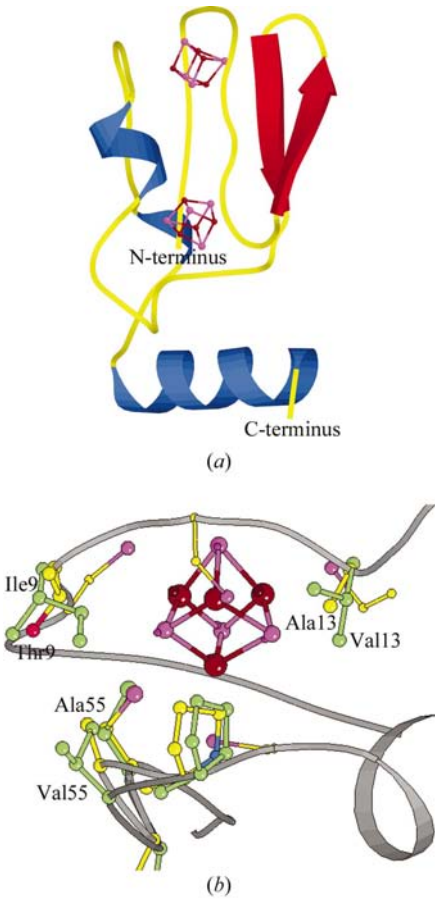

Figure 2
Structure of the ferredoxin of *T. aromatica*. (*a*) Ribbon diagram of the overall fold. (*b*) The surroundings of the low-potential [4Fe–4S] cluster of the superimposed TaFd and CvFd. Only the non-conserved side chains (except for residue 10) in the vicinity of cluster I are presented (CvFd in green) that might cause the different redox potentials. This figure was generated with *MOLSCRIPT* (Kraulis, 1991)

100 and 50 mV, respectively, in line with our interpretation. Interestingly, the exchange of Val55 in CvFd by alanine in TaFd should reduce the potential of the latter, but the superposition of the structures reveals that owing to a different main-chain arrangement the position of the C^{β} atom of Ala55 corresponds to that of the $C^{\gamma 2}$ atom of Val55 in CvFd, which apparently partly compensates for this exchange.

This work was supported by the Max-Planck-Gesellschaft and Deutsche Forschungsgemeinschaft (BO 1565). We thank Georg Fuchs and Hartmut Michel for continuous support and the staff of the Max-Planck beamline at DESY (Hamburg) and the ID14-4 beamline at ESRF (Grenoble) for help during data collection.

References

Adman, E. T., Sieker, L. C. & Jensen, L. H. (1973). *J. Biol. Chem.* **248**, 3987–3996.

Boll, M. & Fuchs, G. (1998). *Eur. J. Biochem.* **251**, 946–954.

Boll, M., Fuchs, G. & Heider, H. (2002). *Curr. Opin. Chem. Biol.* **6**, 604–611.

Boll, M., Fuchs, G., Meier, C., Trautwein, A. X., El Kasmi, A., Ragsdale, S. W., Buchanan, G. & Lowe, D. J. (2001). *J. Biol. Chem.* **276**, 47853–47862.

Boll, M., Fuchs, G., Tilley, G., Armstrong, F. A. & Lowe, D. J. (2000). *Biochemistry*, **39**, 4929–4938.

Brackmann, R. & Fuchs, G. (1993). *Eur. J. Biochem.* **213**, 563–571.

Breese, K., Boll, M., Alt-Mörbe, J., Schägger, J. H. & Fuchs, G. (1998). *Eur. J. Biochem.* **256**, 48–154.

Breese, K. & Fuchs, G. (1998). *Eur. J. Biochem.* **251**, 916–923.

Brünger, A. T., Adams, P. D., Clore, G. M., DeLlano, W. L., Gros, P., Grosse-Kunstleve, R. W., Jiang, J.-S., Kuszewski, J., Nilges, M., Pannu, N. S., Read, R. J., Rice, L. M., Simonson, T. & Warren, G. L. (1998). *Acta Cryst.* D**54**, 905–921.

Buckel, W. & Keese, R. (1995). *Angew. Chem. Int. Ed. Engl.* **34**, 1502–1506.

Chen, K., Bonagura, C. A., Tilley, G. A., McEvoy, J. P., Jung, Y.-S., Armstrong, F. A., Stout, C. D. & Burgess, B. K. (2002). *Nature Struct. Biol.* **9**, 188–192.

Collaborative Computational Project, Number 4 (1994). *Acta Cryst.* D**50**, 760–763.

Dörner, E. & Boll, M. (2002). *J. Bacteriol.* **184**, 3975–83.

Gibson, J. & Harwood, C. S. (2002). *Annu. Rev. Microbiol.* **56**, 345–369.

Hooft, R. W. W., Vriend, G., Sander, C. & Abola, E. E. (1996). *Nature (London)*, **381**, 272.

Jancarik, J. & Kim, S.-H. (1991). *J. Appl. Cryst.* **24**, 409–411.

Jones, T. A., Zou, J. Y., Cowan, S. W. & Kjeldgaard, M. (1991). *Acta Cryst* A**47**, 110–119.

Kissinger, C. R., Gehlhaar, D. K. & Vogels, D. B. (1999). *Acta Cryst.* D**55**, 484–491.

Kraulis, P. J. (1991). *J. Appl. Cryst.* **24**, 946–950.

Kyritsis, P., Hatzfeldt, O. M., Link, T. A. & Moulis, J.-M. (1998). *J. Biol. Chem.* **273**, 15404–15411.

Laskowski, R. A., MacArthur, M. W., Moss, D. S. & Thornton, J. M. (1993). *J. Appl. Cryst.* **26**, 283–291.

Matthews, B. W. (1968). *J. Mol. Biol.* **33**, 491–497.

Moulis, J.-M. (1996). *Biochim. Biophys. Acta*, **1308**, 12–14.

Moulis, J.-M., Sieker, L. C., Wilson, K. S. & Dauter, Z. (1996). *Protein Sci.* **5**, 1765–1775.

Otwinowski, Z. & Minor, W. (1997). *Methods Enzymol.* **276**, 307–326.

Ramachandran, G. N. & Sasisekharan, V. (1968). *Adv. Protein Chem.* **23**, 283–438.

Tschech, A. & Fuchs, G. (1987). *Arch. Microbiol.* **148**, 213–217.